scientific reports

Check for updates

OPEN

An environmentally friendly deep eutectic solvent for CO_2 capture

Ali Asghar Manafpour, Farzaneh Feyzi✉ & Mehran Rezaee

A leading cause of global warming is the increase of carbon dioxide (CO_2) emissions due to anthropogenic activities which prompts an urgent need for substantial reduction. Recently, CO_2 absorption in deep eutectic solvents (DESs) has attracted scientific attention, because of their adaptability compared to traditional ionic liquids and aqueous amine solutions. This study employs the heating method to synthesize DESs using tetrapropylammonium bromide (TPAB) and formic acid (Fa) with molar ratios of TPAB-Fa (1:1) and TPAB-Fa (1:2). Absorption experiments by static method quantified CO_2 solubility in the DESs under varied pressures and temperatures. TPAB-Fa (1:2) at 25.0 °C was the most efficient with the CO_2 solubility of 0.218. Thermodynamic modeling was performed by employing the nonrandom two liquids activity coefficient model and the Peng–Robinson equation of state for the liquid and gas phases, respectively. The Henry's law constant was determined from experimental data. CO_2 physical absorption was confirmed via nuclear magnetic resonance (NMR) and Fourier-transform infrared (FT-IR) analyses. TPAB-Fa (1:2), as the superior DES, exhibited regeneration efficiency of 99% after five absorption/desorption cycles.

Keywords Carbon dioxide absorption, Deep eutectic solvent, Thermodynamic modeling, Tetrapropylammonium bromide, Formic acid, Sustainable regeneration

Consumption of fossil fuels as the primary energy source significantly affects air pollution and the adverse consequences of climate change[1,2]. Carbon capture and storage (CCS) has emerged as a viable approach to mitigate these detrimental effects, including but not limited to the greenhouse effect, global warming, acidification of the oceans, and the spread of diseases and pests[3,4]. The established methods for carbon capture include adsorption[5], absorption[6], membrane separation[7,8], and chemical capture[9]. The absorption of CO_2 is a promising method due to its effectiveness from an economic and operational point of view. Absorption has better long-term performance and a large processing capacity on the industrial scale[10,11]. Aqueous amine solutions are the most frequently used reversible solvents for CO_2 capture in industrial processes[12]. Monoethanolamine (MEA) aqueous solution is extensively utilized in contemporary industries for CO_2 absorption because of its low cost, notable reactivity, high CO_2 capture capacity and significant absorption rate[13]. However, these solvents have some inherent significant drawbacks, such as amine loss due to volatility, environmental issues, high corrosion effects, high energy consumption for the desorption process[14–16] and degradations at high temperatures. Therefore, it is crucial to find environmentally friendly alternatives to aqueous amine-based solvents.

Ionic liquids (ILs) have been the subject of considerable research on CO_2 absorption. This is primarily due to their tunable chemical structure, low vapor pressure, nonflammability, high solvation capacity, thermal stability and potential for utilization at ambient temperature[17–19]. ILs have been found to have applications in various fields, such as organic synthesis, catalysis, separation during extraction and electrochemistry[20]. Numerous subsequent efforts have been devoted to investigating the solubility of CO_2 in ILs. Blanchard et al.[21] conducted the first investigation of CO_2 absorption by 1-butyl-3-methylimidazolium hexafluorophosphate ([Bmim][PF_6]) using a high-pressure cell. [Bmim][PF_6] absorbed a mole fraction of 0.6 CO_2 at a temperature of 25 °C and a pressure of 8 MPa. Bates et al.[22] suggested a new kind of amino group-functionalized IL with a 0.5 molar uptake of CO_2 per mole of IL at a pressure of 1 atm and temperature of 295 K. Huang et al.[23] documented the presence of a chemical reaction between CO_2 and a basic ionic liquid (ethyltributylphosphonium succinimido ([P4442][Suc])). This reaction usually leads to the absorption of CO_2 with capacities ranging from 0.5 to 1 mol of CO_2 per mole of ionic liquid at a temperature of 25 °C and various partial pressures of CO_2. However, ILs encountered several limitations that have precluded them from emerging as an optimal candidate for green solvents, including complex and expensive synthesis and the requirement for high purity because the presence of impurities can significantly impair the physicochemical properties of ILs[24,25].

Thermodynamic Research Laboratory, School of Chemical, Petroleum and Gas Engineering, Iran University of Science and Technology, Tehran 16846-13114, Iran. ✉email: feyzi@iust.ac.ir

More research is also needed to determine if these solvents are environmentally friendly[26–29]. To overcome these drawbacks, while maintaining the beneficial characteristics of ILs, a novel class of solvents called deep eutectic solvents (DESs) has been developed.

DESs are formed by combining a hydrogen bond donor (HBD) with a hydrogen bond acceptor (HBA). Since DESs can easily be synthesized, they are practical and economical alternatives to ILs. The first DES was synthesized by Abbott et al.[30] using choline chloride (ChCl) and urea with the molar ratio of 1:2. Both of these components are biodegradable and non-toxic. Some of recent investigations have focused on the corrosion behavior of DES based on choline chloride, representing ammonium quaternary salts. These studies have recognized the high stability of the ammonium salt, which can maintain its stability without decomposition or deactivation under severe electrochemical conditions and in the presence of negative electrical potentials. Consequently, a considerable body of literature exists on the application of choline chloride-based DESs as corrosion inhibitors in aqueous environments[31]. Ammonium quaternary salts are the most commonly employed HBAs due to their accessibility, affordability and low toxicity[32,33]. Another advantage of DESs is that HBD and HBA concentrations may be modified to customize their properties for a specific purpose[34–37]. Also, DESs have emerged as a viable substitute for ILs for CO_2 absorption[38–41]. Li et al.[42] effectively synthesized several choline-based DESs and utilized them for CO_2 absorption for the first time. They demonstrated that at a pressure of 12.5 MPa and a temperature of 40 °C, ChCl-urea (1:2) absorbed CO_2 with a mole fraction of 0.309. Leron et al.[43] investigated the impact of varying temperatures and pressures on the CO_2 solubility in ChCl-urea (1:2) at temperatures ranging from 303.15 to 343.15 K and pressures of up to 6.0 MPa. They demonstrated that CO_2 solubility in ChCl-urea (1:2) DES increased with increasing pressure and decreased with increasing temperature. Additionally, they examined how the molar ratio of salt and HBD affects the solubility of CO_2. The solubility of CO_2 in various ammonium and phosphonium DESs was examined by Sarmad et al.[44] at temperatures of 298.15 K and pressures of up to 2 MPa. They reported that the CO_2 solubility of 15 synthesized DESs is higher than that of conventional ILs. It should be mentioned that the renewal of the absorbent in practical applications is important in any absorption process including CO_2 capture. Zhang et al.[45] demonstrated that after six absorption–desorption cycles, the regeneration efficiency of [TETA]Cl-DG (1:2) and [TETA]Cl-EG (1:3) drops from 100 to 97.5%. Yan et al.[46] examined the solubility of CO_2 in various superbase IL-based DESs. The 1,8-diazabicyclo-[5,4,0] undec-7-ene imidazole/Ethylene glycol ([HDBU][Im]/EG) with a mass ratio of 7:3, exhibited the maximum CO_2 absorption capacity of 0.141 g CO_2 per g DES at 100 kPa and 40 °C. Additionally, the CO_2 absorption capacity of DES remained stable after five absorption and desorption cycles. Recently, several articles have investigated the effect of viscosity on the solubility of CO_2 in DESs[47,48]. The solvent's viscosity is an important physical property that can substantially impact the mass transfer[49]. An enhancement in the solvent's capacity to capture CO_2 can result from a reduction in viscosity[50]. Viscosity, also, impacts the energy needed to manufacture and move materials[51]. Temperature, kind of HBA and HBD, and their respective molar ratios all affect the viscosities of DESs[52]. The viscosity of DES increases during absorption, resulting in a decrease in the absorption rate[46,49]. Some studies have documented the viscosities of amine-based DESs in their pure form and the viscosities of the DESs after CO_2 absorption[45,53]. For a solvent to be considered suitable in the gas absorption industry, multiple factors beyond absorption capacity must be evaluated. For solvents with relatively low toxicity, considerations include the potential for long-term use, the absence of solvent loss, the energy required for solvent recovery, and the regenaration efficiency after multiple absorption and desorption cycles. Aqeous amine solutions which chemically absorb CO_2, present challenges such as low biodegradability, volatility, and high energy requirements for regeneration, which are costly and environmentally detrimental.

Our study is focuses on experimentally investigating the utilization of tetrapropylammonium bromide (TPAB) and a naturally occurring carboxylic acid to form a DES for CO_2 capture. To accomplish this goal, two DESs were synthesized employing TPAB as a hydrogen bond acceptor (HBA) and formic acid (Fa) as a hydrogen bond donor (HBD) in molar ratios of 1:1 and 1:2. The presence of hydrogen bond between TPAB and Fa, and physical absorption of CO_2 were confirmed through FT-IR and NMR spectra. Experiments were conducted at the temperatures of 25.0, 35.0 and 45.0 °C and pressures of approximately up to 35.000 bar. The impact of variations in pressure, temperature, and viscosity on CO_2 absorption was investigated. Using the CO_2 solubility data, Henry's law constant and the enthalpy of dissolution were obtained. To model the vapor–liquid equilibrium of the CO_2-DES system, the Peng–Robinson equation of state (PR EOS)[54] and the nonrandom two liquid (NRTL)[55] activity coefficient model were employed. Furthermore, five cycles of regeneration experiments were performed on the DES with better performance under vacuum and at 65.0 °C condition.

Experimental procedure

Materials

The substances used in this study and their corresponding molecular structures, sources, and purities are presented in Table 1. They were used as received.

Synthesis of DESs

The DESs were synthesized by the heating method. HBA and HBD were mixed at a precise molar ratio and temperature. TPAB and Fa were introduced into a stainless steel two-shell reactor autoclave. Two DESs were made with the molar ratios of TPAB-Fa (1:1) and TPAB-Fa (1:2) using a balance (Precisa XT220A with the precision of $\pm 10^{-4}$ g). The mixture was then agitated using a magnetic stirrer (Fisher, Cat. No. 14–511-113) and heated using a circulating water bath (LAUDA Alpha RA 8, 248–373 K) for five hours at 70.0 °C. The obtained liquid was a clear and uniform phase.

Chemicals	Sources	Purities/wt%	Molecular structure
Tetrapropylammonium bromide (TPAB)	Sigma–Aldrich	≥98	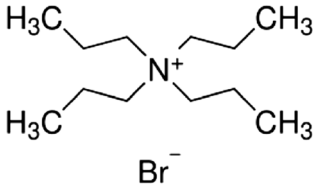
Formic acid (Fa)	Daejung	≥99	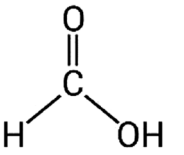
Carbon dioxide (CO_2)	Roham Gas Company	≥99	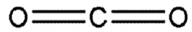

Table 1. Names of chemicals and their purities used in this study.

CO_2 absorption experimental setup

The equipment used for the absorption experiments, which is shown in Fig. 1, is the same as used in the author's previous publications[56–59]. It is comprised of a CO_2 gas cylinder, a gas container (182 ml) connected to the CO_2 cylinder via valve V_1, an autoclave reactor (37 ml) connected to the gas container through valves V_4 and V_6, a magnetic stirrer (Fisher, Cat. No. 14–511-113), a circulating water bath (LAUDA Alpha RA 8, 248–373 K) for temperature adjustment, temperature sensors (T_{S1}, T_{S2}) (K-type, with the precision of ± 0.1 K), and pressure sensors (P_{S1}, P_{S2}) (Sensys, Model: M5156-11700X-050BG, with the precision of ± 2.5 kPa). These sensors measure and control the temperature and pressure of the gas container and autoclave reactor. They are connected to a computer for data analysis, display, and storage. V_2, V_7, and V_8 are the valves that release CO_2 from the system. V_3 and V_5 valves connect the gas container and autoclave reactor to P_{S1} and P_{S2}.

FT-IR, NMR, and viscosity analyses

To investigate the hydrogen bond interaction between HBA and HBD and the production of DES, we employed analytical techniques such as FT-IR (Perkin Elmer Spectrum RX1, Canada) and NMR (Bruker DRX-500, operating at 500 MHz). Furthermore, to determine the absorption mechanism, these investigations were carried out before and after CO_2 absorption. The viscosity of the eutectic solvent was measured using the dynamic shear rheometer (DSR) SmartPave 102e at temperatures of 25.0 and 45.0 °C for each molar ratio of DES.

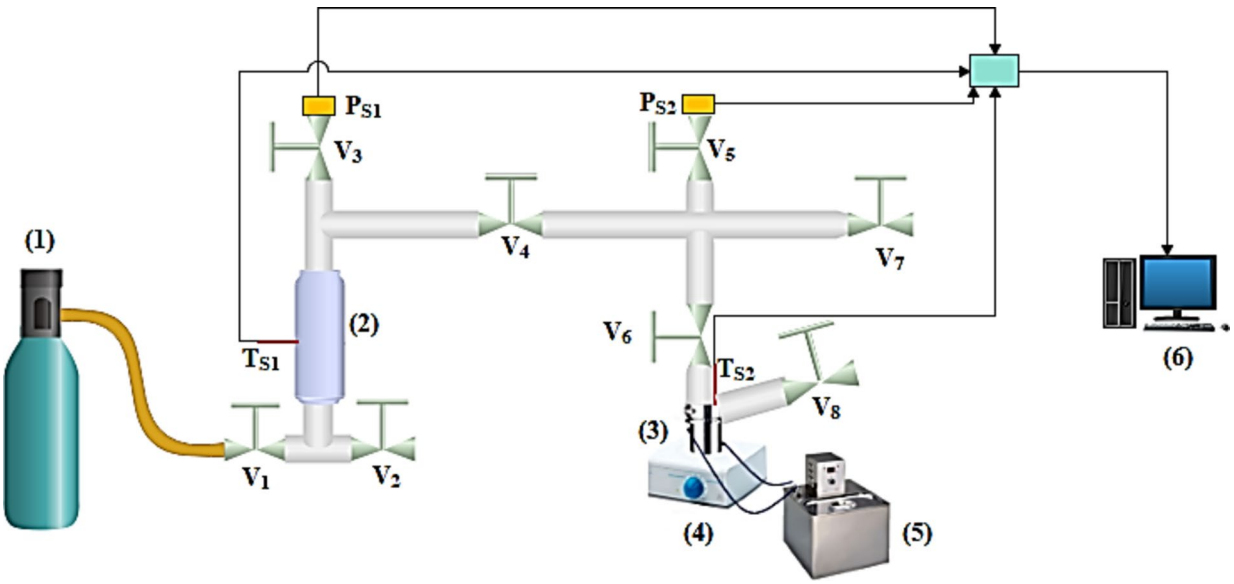

Fig. 1. Schematic of the experimental setup for CO_2 absorption–desorption: (1) CO_2 cylinder, (2) gas container, (3) autoclave reactor, (4) magnetic stirrer, (5) circulating water bath, and (6) computer.

CO_2 absorption and desorption experiments

A precise amount of DES was injected into the autoclave reactor, then, the gas container and the autoclave reactor were purged of gases using a vacuum pump. CO_2 was supplied into the gas container from the cylinder. After the temperature and pressure of the gas container were fixed, the quantity of CO_2 entering the gas container ($n^e_{co_2}$) was determined by applying Eq. (1). Subsequently, CO_2 was delivered into the autoclave reactor. Equations (2), (3) were employed to calculate the number of moles of CO_2 that remained in the CO_2 container ($n^r_{co_2}$) and entered into the autoclave reactor ($n^g_{co_2}$).

$$n^e_{CO_2} = \frac{P_e V_{gc}}{Z^e_{CO_2} R T_e} \tag{1}$$

$$n^r_{CO_2} = \frac{P_r V_{gc}}{Z^r_{CO_2} R T_r} \tag{2}$$

$$n^g_{CO_2} = n^e_{CO_2} - n^r_{CO_2} = \frac{V_{gc}}{R}\left(\frac{P_e}{Z^e_{CO_2} T_e} - \frac{P_r}{Z^r_{CO_2} T_r}\right) \tag{3}$$

In the above equations P, T, and Z represent pressure, temperature, and compressibility factor, respectively. Superscripts and subscripts e and r refer to entering and remaining in the gas container, respectively. $n^g_{CO_2}$ denotes the number of gas molecules entering the autoclave reactor. R and V_{gc} represent the universal gas constant and the volume of the gas container, respectively. Equations (4), (5) were employed to calculate the amount of CO_2 molecules absorbed in the DES ($n^l_{CO_2}$) and the amount that remained in the autoclave reactor after reaching equilibrium ($n^{eq}_{CO_2}$). Superscript eq refers to the phase equilibrium condition, V_{DES} refers to the volume of the solvent and V is the volume of the autoclave reactor.

$$n^l_{CO_2} = n^g_{CO_2} - n^{eq}_{CO_2} \tag{4}$$

$$n^{eq}_{CO_2} = \frac{P^{eq}_{CO_2}(V - V_{DES})}{Z^{eq}_{CO_2} R T^{eq}_{CO_2}} \tag{5}$$

All the compressibility factors were calculated by the PR EOS[54].

CO_2 absorption investigations were conducted at three temperatures (25.0, 35.0, and 45.0 °C) and, as mentioned before, two TPAB to Fa molar ratios of 1:1 and 1:2. Six equilibrium pressures (ranging from 1.650 to 35.125 bar) were determined at each temperature for each TPAB to Fa molar ratios. Five regeneration cycles were conducted at 65.0 °C and atmospheric pressure for the best TPAB to FA ratio, which is specified in the next sections. The efficiency of solvent regeneration (η_{reg}) was determined using Eq. (6) in which the number of moles of CO_2 absorbed during the i-th regeneration and the initial absorption are represented by the variables n_i and n_0, respectively.

$$\eta\% = \frac{n_i}{n_0} \tag{6}$$

CO_2 absorption thermodynamic modeling

The γ-φ approach was adopted for thermodynamic modeling. The solubility of CO_2 was determined by using the NRTL[55] model in conjunction with the PR EOS. The PR EOS[54] is presented by Eqs. (7), (8), (9), (10).

$$P = \frac{RT}{v - b} - \frac{a}{v(v + b) + b(v - b)} \tag{7}$$

$$a = \frac{0.45724(RT_C)^2}{P_C}\left[1 + m(1 - T_r{}^{0.5})\right]^2 \tag{8}$$

$$b = 0.0778\frac{RT_C}{P_C} \tag{9}$$

$$m = 0.37464 + 1.5422\omega - 0.2699\omega^2 \tag{10}$$

where a is the parameter representative of attractive forces between molecules and b denotes the co-volume parameter. v, T_C, P_C, ω, and T_r are the volume, the critical temperature, the critical pressure, the acentric factor, and reduced temperature, respectively. Equations (11), (12), (13) represent the NRTL[55] activity coefficient model.

$$ln\gamma_i = \frac{\sum_j x_j \tau_{ji} G_{ji}}{\sum_k x_k G_{ki}} + \sum_j \frac{x_j G_{ji}}{\sum_k x_k G_{ki}} + \left(\tau_{ij-} \frac{\sum_m x_m \tau_{mj} G_{mj}}{\sum_k x_k G_{kj}}\right) \tag{11}$$

$$G_{ij} = \exp(-\alpha\tau_{ji}) \tag{12}$$

$$\tau_{ji} = \frac{b_{ji}}{RT} \tag{13}$$

α and b_{ji} are the non-randomness and binary interaction parameters, respectively.

Results and discussion

Structure of DESs

FT-IR analysis of synthesized DESs

Figure 2 displays the FT-IR spectra of Fa, TPAB, TPAB-Fa (1:1), and TPAB-Fa (1:2). The spectra of Fa exhibits two peaks at 2941 and 3106 cm^{-1}, which are attributed to the –OH stretching vibration[29,60]. In contrast, the spectra of TPAB shows peaks at 2870, 2926, and 2963 cm^{-1}, which are related to the -CH stretching vibration[61]. After blending the substances, the spectral peaks at 2941 cm^{-1} and 3106 cm^{-1} of Fa and the peak at 2926 cm^{-1} of TPAB are eliminated for both DESs. The removal can be attributed to the establishment of hydrogen bonds between TPAB and Fa. Furthermore, the TPAB peaks at 2870 and 2963 cm^{-1} have shifted to 2960 and 2975 cm^{-1}, respectively, with decreased intensity. This phenomenon can be attributed to a modification in the intensity of the hydrogen bonds. The combination of two separate peaks at 1458 and 1487 cm^{-1} in the TPAB spectrum into a solitary peak at 1476 cm^{-1}, detected in the spectra of both DESs, provides more insight into the creation of hydrogen bond[62].

NMR analysis

The ^{1}HNMR and ^{13}CNMR spectra of HBA, HBD, and DES were obtained using deuterium oxide (D_2O) as the solvent. Figure 3 displays the ^{1}HNMR spectra of Fa, TPAB, and TPAB-Fa (1:2). TPAB-Fa (1:2) was subjected to ^{13}CNMR and ^{1}HNMR analysis as the superior DES for CO_2 absorption. Upon mixing, it is evident that the peak of Fa at $\delta = 7.41$ ppm, associated with the –CH group, has shifted to $\delta = 8.11$ ppm, showing a change of the C–H bond in Fa as an HBD. However, the change in the peak at $\delta = 4.85$ ppm, related to D_2O, is insignificant[63]. The peak related to OH has been removed due to the presence of D_2O in the system. Fa and TPAB have formed a hydrogen bond connection using the hydrogen atom in the OH group of Fa. Furthermore, the TPAB exhibits peaks at $\delta = 3.11$, 3.17, and 1.72 ppm, which have shifted to 2.98, 1.51, and 0.77 ppm, respectively. This shift indicates that the C–H stretching of TPAB, as a hydrogen bond acceptor, has changed. Based on the explanations provided, it can be deduced that Fa and TPAB effectively carried out their roles as the HBD and HBA, respectively. A primary concern in application of the resulting eutectic solvent in gas absorption, is its potential release into

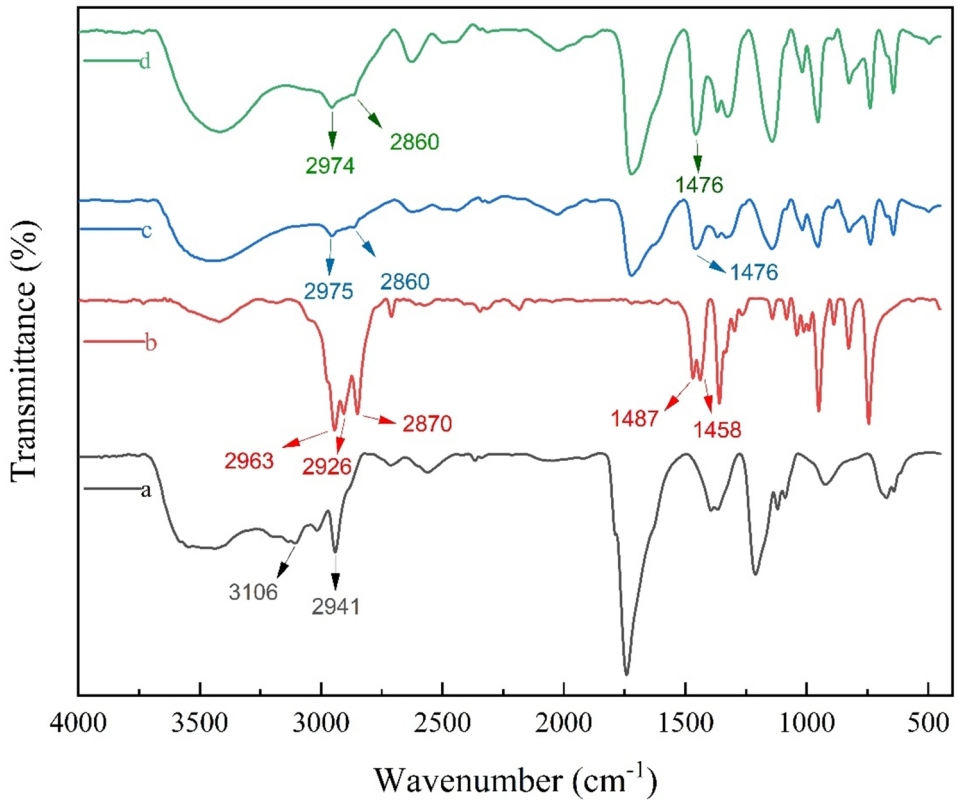

Fig. 2. FT-IR spectra of HBA, HBD, and DESs. (**a**) Fa, (**b**) TPAB, (**c**) TPAB-Fa (1:1), (**d**) TPAB-Fa (1:2).

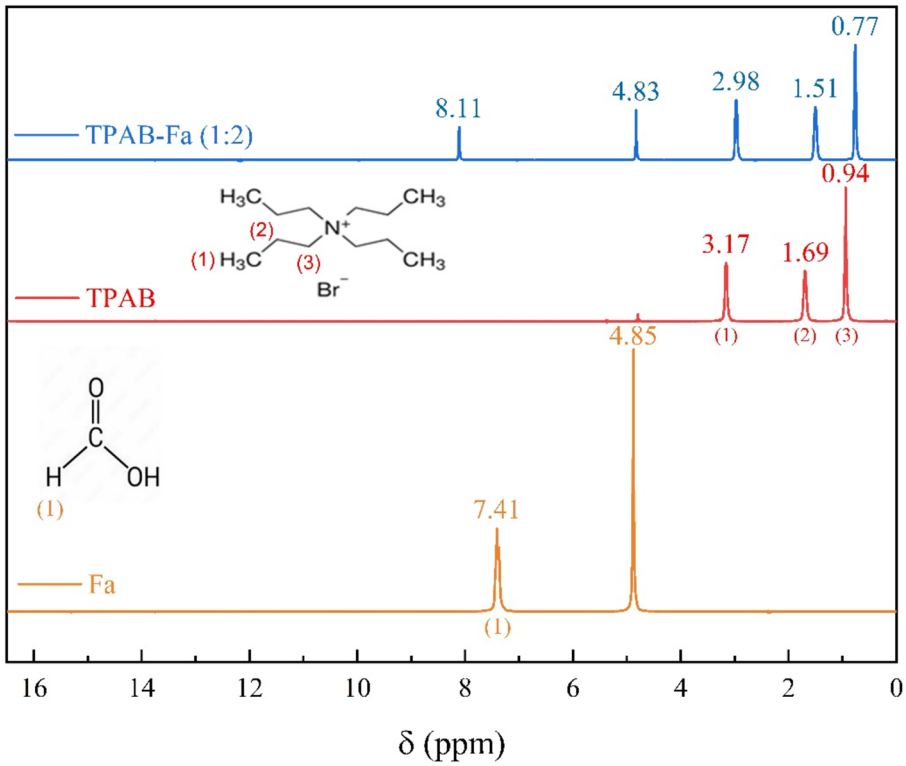

Fig. 3. ^{1}HNMR spectra of Fa, TPAB, TPAB-Fa (1:2).

the environment. NMR and FTIR analyses of the raw materials and the DES indicate that hydrogen bonds form between the raw materials without any chemical reactions. This characteristic reduces the solvent's volatility that significantly diminishes the risk of atmospheric dissemination.

CO_2 solubility

The results of CO_2 solubility at three different temperatures, two molar ratios of HBA to HBD, and six pressures are shown in Fig. 4. It is observed that the molar fraction of CO_2 increases by increase in pressure and decreases with increasing temperature. Initially, the impact of the HBA to HBD molar ratio was examined, which showed that the CO_2 solubility of TPAB-Fa (1:2) was higher than that of TPAB-Fa (1:1) at the same temperature. The TPAB-Fa (1:2) had the maximum CO_2 absorption (x_{CO_2}) at pressures higher than 30.000 bar and temperatures of 25.0, 35.0, and 45.0 °C, with values of 0.218, 0.156, and 0.137, respectively, whereas the TPAB-Fa (1:1) showed solubility values of 0.169, 0.147, and 0.127 at the same temperatures. Higher absorption in the TPAB-Fa (1:2) could be attributed to the existence of more location for CO_2 absorption because of one more –OH group, as shown by the ^{1}HNMR study, which also revealed that TPAB and Fa had a hydrogen bond from the –OH side of Fa.

Furthermore, the justification for this observation can be the viscosity of DESs. As mentioned previously, the viscosity of any solvent plays a crucial role in absorption. The viscosity values of TPAB-Fa (1:2) at 25.0 and 45.0 °C are 53.98 and 21.62 mPa·s, respectively, whereas the viscosity of TPAB-Fa (1:1) are 946.16 and 222.55 mPa·s at the same temperatures. As the HBD ratio increased, the eutectic solvent viscosity decreased.

Our results showed that the solvation of CO_2 in the DES with the higher HBD to HBA ratio was higher at the same temperature. In other words, the relationship between viscosity and temperature is inversely proportional. Higher temperatures lead to less absorption, whereas lower viscosities increase the solubility of CO_2. At 25.0 and 35.0 °C temperatures, TPAB-Fa (1:1) demonstrated more capture than TPAB-Fa (1:2) at temperatures of 35.0 and 45.0 °C, respectively. This suggests that the impact of temperature outweighs the impact of viscosity. Figure 4 also demonstrates that the difference in CO_2 absorption at varying temperatures under low pressures is negligible.

Nevertheless, with increasing pressure, the effect of temperature on absorption becomes more significant. Desorption of CO_2 may be done by lowering pressure to a vacuum and relying less on raising temperature to high levels. The desorption operation can make advantage of this observation to achieve high desorption efficiency with less energy consumption.

The absorption process mechanism was identified by FT-IR and ^{13}CNMR analyses. Figure 5 presents the FT-IR analysis of DESs before and after CO_2 absorption. A small new peak at 2200 cm^{-1} is observed after absorption in TPAB-Fa (1:1); indicating the presence of asymmetric O = C = O stretching in the eutectic solvent. In addition, considerable peaks are seen at 3600–3800 cm^{-1}, identifying CO_2 combination bands[64,65]. These combination bands arise from the interactions between different vibrational modes, enhancing the utility of FTIR spectroscopy in studying and quantifying CO_2 in diverse applications[65]. No substantial change is observed in peaks of TPAB-Fa

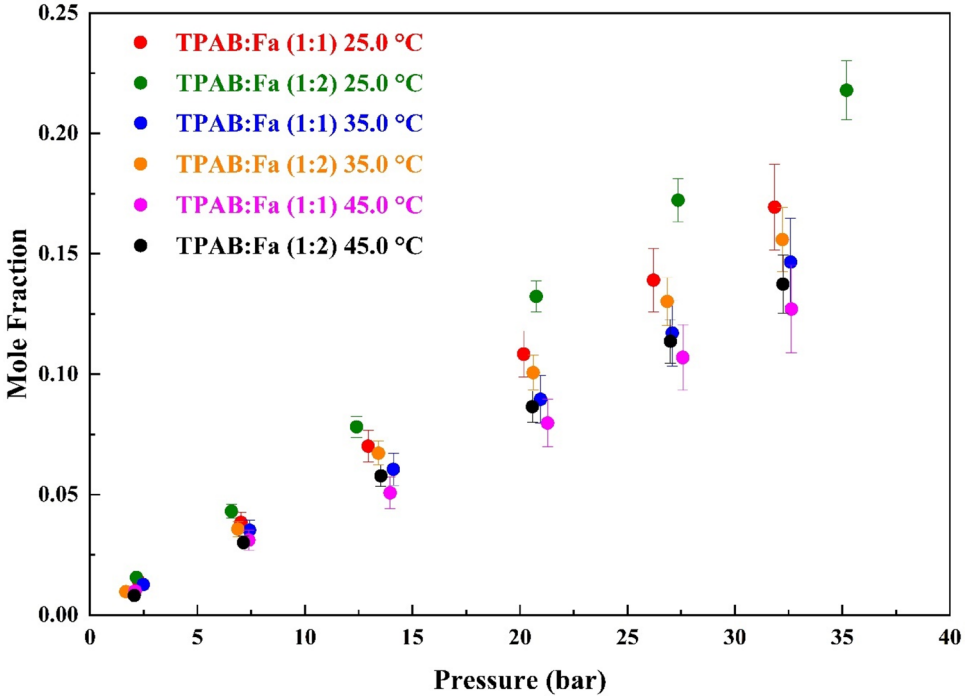

Fig. 4. Experimental mole fraction of absorbed CO_2 in two molar ratios of DES at 25.0, 35.0, and 45.0 °C and pressures up to 35.000 bar.

(1:2) after absorption. This may be due to the low viscosity of the DES, which causes CO_2 to desorb quickly before FT-IR and NMR analyses can be conducted, also indicating no chemical reactions between the DES and CO_2. This issue was further validated by the ^{13}CNMR analysis depicted in Fig. 6. It is evident that after absorption, both the number and quantity of ^{13}CNMR peaks are not changed in TPAB-Fa (1:2), suggesting that the CO_2 was absorbed physically[66]. We may reach to the conclusion that it is due to the physical nature of the absorption mechanism that absorption amount increases with increasing pressure.

Thermodynamic modeling of vapor–liquid equilibrium

The DES-CO_2 phase equilibrium was correlated using PR EOS[54] and NRTL model[55] for the vapor and liquid phases, respectively. It was assumed that the experimental vapor pressure of DES is negligible. Hence, the vapor phase consists of pure CO_2. Henry's law constant was calculated using the slope of the fugacity-mole fraction diagram of experimental data at points where the mole fraction was less than 0.08. The γ-φ approach was used to fit the NRTL[55] binary interaction parameters. The value of α was set to 0.3. Parameters were adjusted using the MATLAB[67] software (version 2022b 1.0.0.1) for both DESs at each temperature. The objective function (OF) was defined by Eq. (14).

$$\mathrm{OF\%} = min\left(\frac{\sum_{i=1}^{n}(\left|x_{iexp} - x_{ical}\right|)}{n}\right) \times 100 \tag{14}$$

where n represents the number of data points. x_{exp} and x_{cal} denote the experimental and calculated mole fractions, respectively. Table 2 introduces the Henry's law constants, OF, (b_{ij}, b_{ji}).

In Fig. 7, the modeling results of the γ-φ approach and the experimental solubility data are compared. As it is observed, the calculation results are extremely close to the experimental data.

Desorption of CO_2

Critical considerations when identifying stable solvents for industrial applications require the degree to which the solubility decreases after a series of absorption–desorption steps. Based on the data presented in Fig. 4, there is no significant difference in CO_2 absorption at low pressures between 25.0 and 45.0 °C. Therefore, it can be inferred that in the desorption process, which occurs at higher temperatures and lower pressures, the temperature increase does not play a significant role in desorption compared to the pressure decrease. In contrast to previous studies that considered a desorption temperature of 100°C[66,68,69], this study reached high desorption efficiency at approximately vacuum pressure and a temperature of 65.0 °C. This practical study demonstrates high desorption efficiency at a temperature considerably lower than other studies. The mole fraction of CO_2 in TPAB-Fa (1:2) is shown in Fig. 8 after six successive absorptions at 25.0 °C and desorption at 65.0 °C in vacuum condition. During the initial absorption after regeneration, the solvent's efficiency decreased by approximately

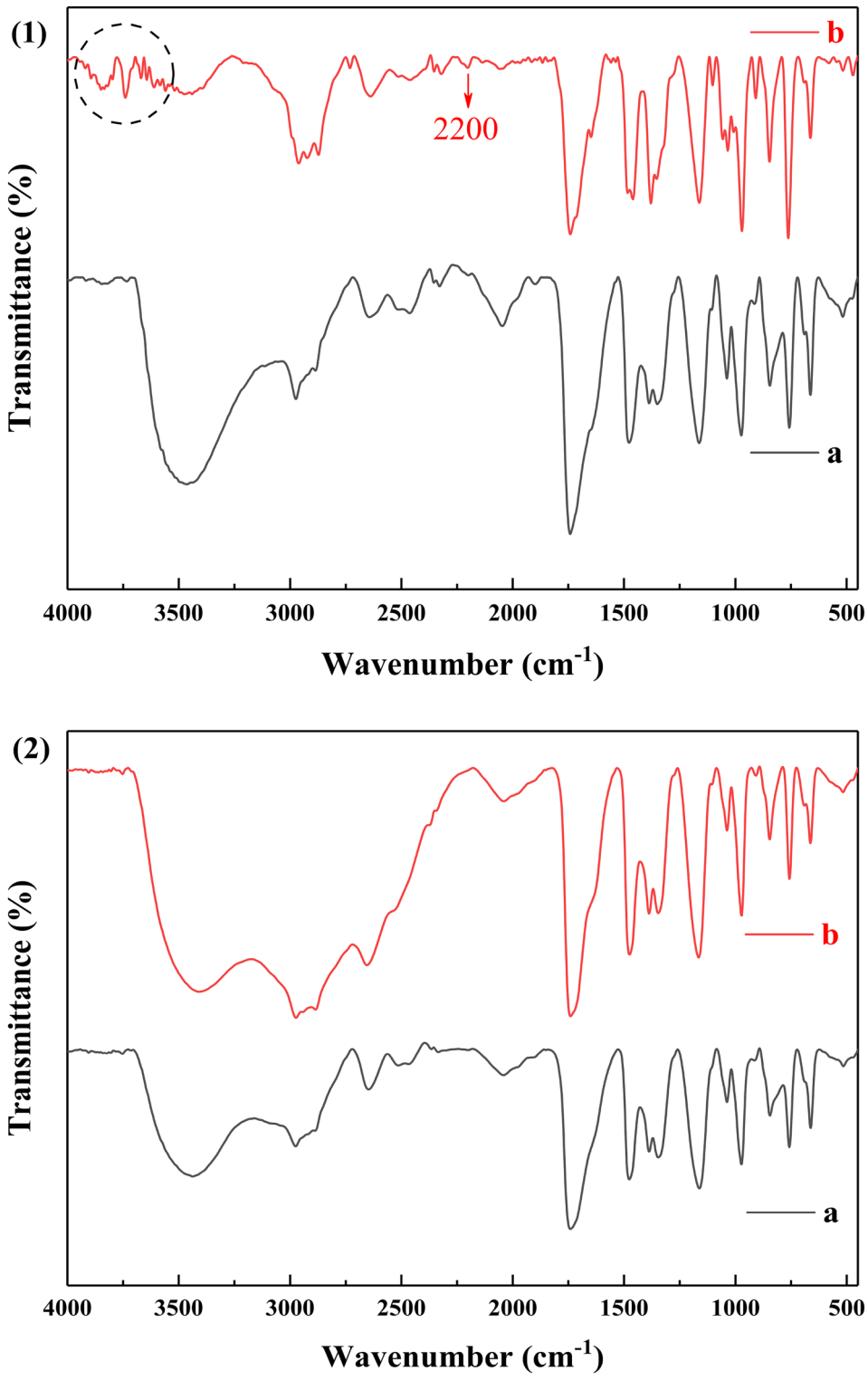

Fig. 5. FT-IR analysis of DES before and after absorption: (**a**) before absorption, (**b**) after absorption, (1) TPAB-Fa (1:1), (2) TPAB-Fa (1:2).

1% at the maximum pressure. The amount of experimental CO_2 absorption during the second to fifth cycle, at the same pressures as the first absorption–desorption cycle, was determined using regression between values of pressure. However, the solvent's efficiency remained relatively stable in the subsequent four cycles. Table 3 displays regeneration efficiency (η_{reg}) of DESs at each cycle. At low pressures, the percentage was approximately 90–95%. However, as the pressure increased, the percentage also increased. Eventually, at the highest pressure, regeneration

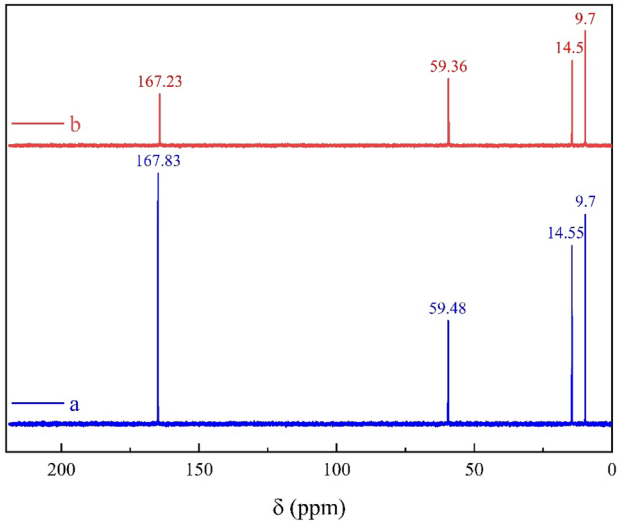

Fig. 6. ^{13}CNMR analysis of TPAB-Fa (1:2), (**a**) before absorption, (**b**) after absorption.

Component *i*	b_{ij}/(J/mol)	b_{ji}/(J/mol)	Henry's law constant /Mpa	OF %
TPAB-Fa (1:2) 25.0 °C	4701.31	−947.23	15.09	0.06
TPAB-Fa (1:2) 35.0 °C	2835.88	−1124.47	18.92	0.09
TPAB-Fa (1:2) 45.0 °C	3133.29	−1531.50	21.51	0.20
TPAB-Fa (1:1) 25.0 °C	5875.29	−916.57	17.51	0.11
TPAB-Fa (1:1) 35.0 °C	4366.95	−526.91	22.30	0.21
TPAB-Fa (1:1) 45.0 °C	2758.89	624.14	26.96	0.15

Table 2. Calculated Henry's law constant and NRTL parameters for the DES-CO_2 system, assuming $\alpha = 0.3$, component *j* is CO_2.

efficiency was 99%, demonstrating the low volatility and high stability of the resulting DES. Additionally, the high reversibility of this DES minimizes the need for replenishment.

Comparison to other DESs

Table 4 presents the solubility of CO_2 in several DESs at varying pressure and temperature ranges compared to the DESs utilized in this study. The findings indicated that TPAB-Fa (1:2) and TPAB-Fa (1:1) outperformed most other solvents. Moreover, it should be taken into account that formic acid is an affordable organic acid with minimal risks to humans and environment due to its natural character. Similarly, TPAB is a cost-effective quaternary ammonium salt. Consequently, the chemicals used in preparing these DESs are more economical than most commonly employed substances in other DESs.

To determine the energy required for the process and the subsequent recovery of the solvent, it is necessary to estimate the enthalpy of solvation (ΔH_{sol}), defined as the strength of the intermolecular interaction between DES and CO_2. The ΔH_{sol} was determined at a fixed mole fraction ($x_{CO_2} = 0.1$) using the Clausius–Clapeyron equation at 25.0 to 45.0 °C. The results are presented in Table 5. This is then compared to several other DESs and solvents.

$$\Delta H_{sol} = R\left(\frac{\partial \ln P}{\partial\left(\frac{1}{T}\right)}\right)_{x_{CO_2}} \tag{15}$$

Due to the negative values of ΔH_{sol}, the absorption process of DESs is exothermic. This is the reason why the absorption amount decreases with increasing temperature. While the values of ΔH_{sol} are within the range of other physical and chemical solvents, they are notably lower than aqueous MEA solution. This behavior suggests a weaker interaction between CO_2 and DES molecules, resulting in improved regeneration capability for the DESs used in this study. In other words, the DES requires less energy for the regeneration process, which leads to a reduction in the consumption of non-renewable energy sources and a reduction in the environmental impact caused by their consumption.

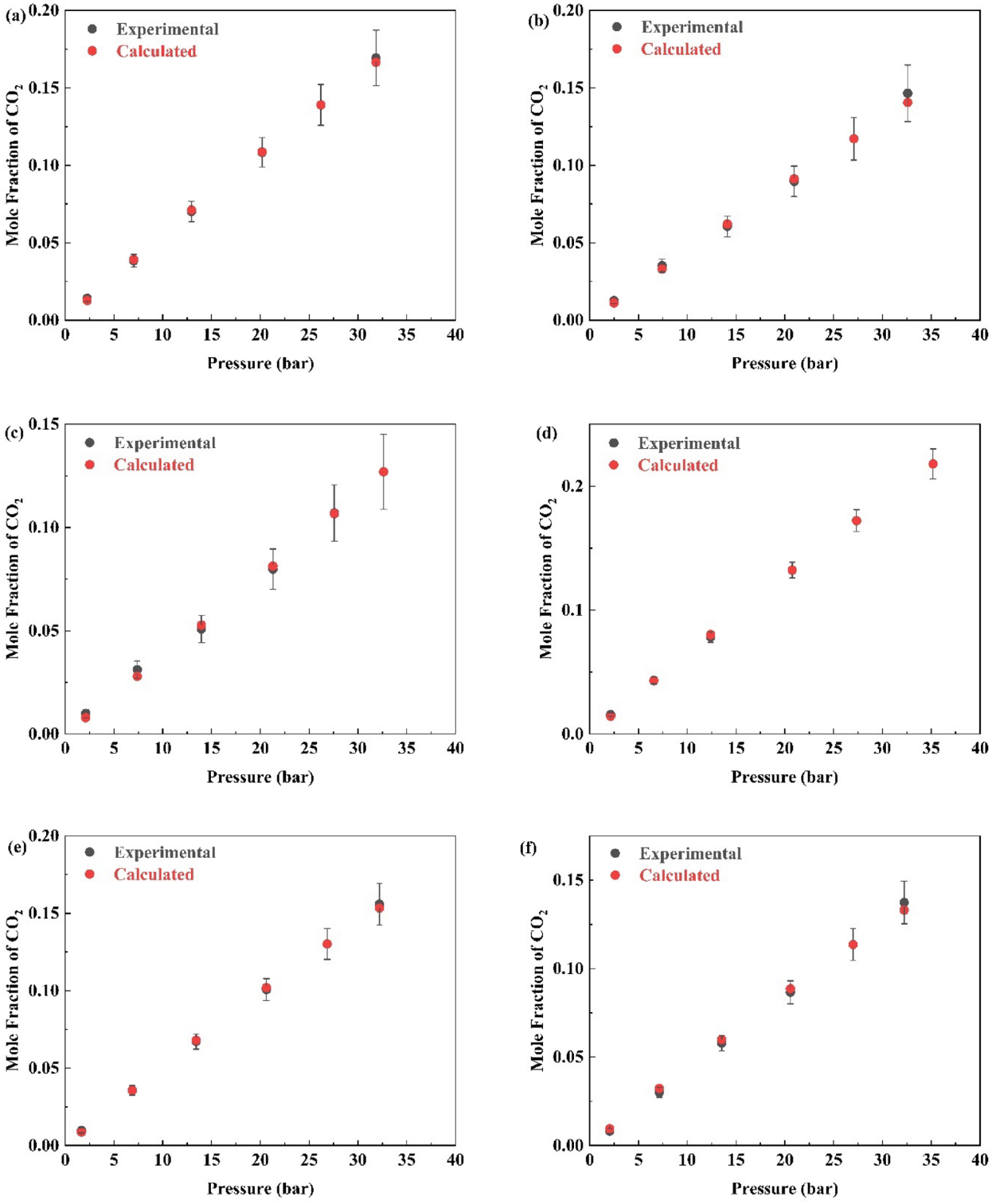

Fig. 7. Calculated and experimental mole fractions as a function of pressure at different temperatures: (**a**) TPAB-Fa (1:1) at 25.0 °C, (**b**) TPAB-Fa (1:1) at 35.0 °C, (**c**) TPAB-Fa (1:1) at 45.0 °C, (**d**) TPAB-Fa (1:2) at 25.0 °C, (**e**) TPAB-Fa (1:2) at 35.0 °C, (**f**) TPAB-Fa (1:2) at 45.0 °C.

Conclusions

This research aimed to investigate the CO_2 absorption capacity of TPAB-Fa (1:1) and TPAB-Fa (1:2) DESs at three different temperatures (25.0, 35.0, and 45.0 °C) and pressures up to more than 35.000 bar. The FT-IR spectra validated the hydrogen bond between HBA and HBD and confirmed the physical absorption of CO_2 in DES.

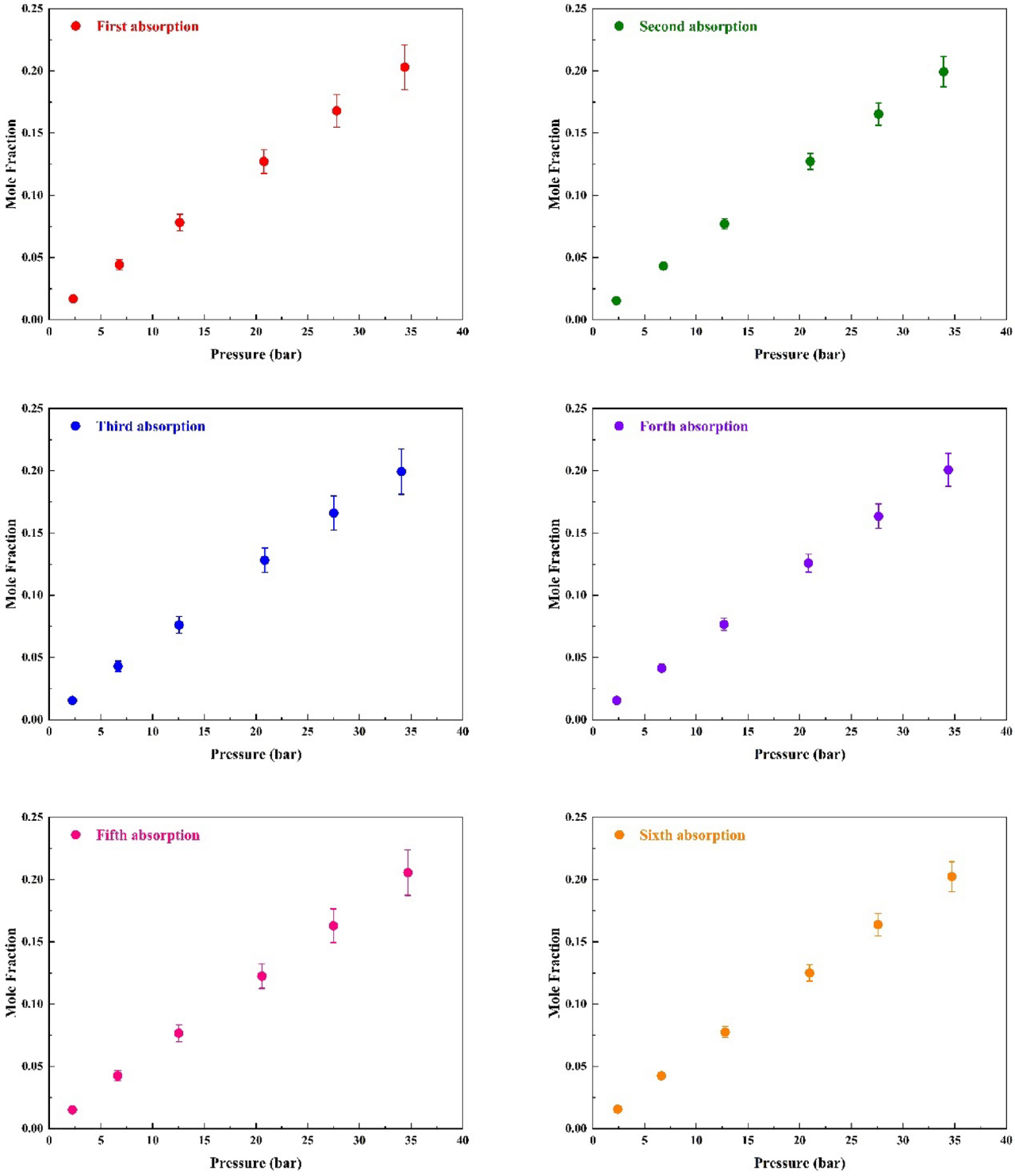

Fig. 8. TPAB-Fa (1:2) absorption–desorption cycle: absorption at 25.0 °C and approximately 2.000–35.000 bar, desorption at 65.0 °C and under vacuum.

TPAB-Fa (1:2) demonstrated the highest CO_2 solubility ($x_{CO_2} = 0.218$) at 25.0 °C and the pressure of 35.200 bar. The solubility of CO_2 displayed an inverse relation with temperature and viscosity while exhibited a direct relation with pressure. The NRTL activity coefficient model and PR EOS accurately modeled the experimental CO_2 solubility data. Henry's law constant was obtained from experimental data at each temperature. Its minimum value of 15.09 MPa was related to TPAB-Fa (1:2) + CO_2 mixture at 25.0 °C, showing the maximum solubility. The TPAB-Fa (1:2) solvent was regenerated five times under vacuum conditions at 65.0 °C, resulting in a marginal 1% decrease in efficiency. The Clausius–Clapeyron equation was employed to calculate the ΔH_{sol}. According to the values of ΔH_{sol}, the exothermic nature of CO_2 absorption was proved. We may conclude that this study has

Pressure/bar	η_{reg} %				
	First regeneration	Second regeneration	Third regeneration	Forth regeneration	Fifth regeneration
2.325	94.295	96.419	91.435	92.379	89.587
6.775	95.182	95.390	94.238	96.756	96.014
12.625	98.655	99.410	97.950	98.796	98.727
20.775	98.767	97.912	98.032	97.338	97.626
27.800	98.975	99.776	98.253	97.894	97.747
34.400	99.499	99.037	98.897	99.302	99.107

Table 3. Regeneration efficiency (%) at 65.0 °C of TPAB-Fa (1:2) for each cycle of DES recovery at the six pressure steps.

DES (HBA + HBD)	Temperature range (K)	Pressure range (bar)	CO_2 solubility range (mole fraction)	CO_2 solubility range ($kg \cdot mol^{-1}$)	Ref
TBAC + decanoic acid (1:2)	298.15 – 323.15	0.900 – 19.900		0.0420 – 1.5200	[66]
TEAC + levulinic acid (1:3)	303.15 – 333.15	0.661 – 5.854	0.0028 – 0.0340		[70]
TEAB + levulinic acid (1:3)	303.15 – 333.15	0.687 – 5.878	0.0030 – 0.0324		[70]
TBAC + levulinic acid (1:3)	303.15 – 333.15	0.632 – 5.916	0.0040 – 0.0453		[70]
TBAB + levulinic acid (1:3)	303.15 – 333.15	0.702 – 5.864	0.0038 – 0.0432		[70]
TBAC + lactic acid (1:3)	298 – 318	0.940 – 19.930	0.0023 – 0.0618		[71]
TBAC + lactic acid (1:2)	298 – 318	0.930 – 19.920	0.0031 – 0.0761		[71]
TEAC + lactic acid (1:2)	298 – 318	0.940 – 19.930	0.0056 – 0.1551		[71]
TMAC + lactic acid (1:2)	298 – 318	0.930 – 19.930	0.0054 – 0.1403		[71]
TBAB + acetic acid (1:2)	298.15	3.880 – 20.110		0.1400 – 1.1300	[44]
TPAC + ethanolamine (1:4)	298.15	4.810 – 20.090		0.3400 – 1.4300	[44]
TPAC + acetic acid (1:6)	298.15	3.500 – 20.300		0.2500 – 1.7200	[44]
TBAC + acetic acid (1:2)	298.15	3.480 – 20.020		0.1800 – 1.4100	[44]
ChCl + phenol (1:4)	293.15 – 323.15	1.082 – 5.291	0.0024 – 0.0208		[72]
ChCl + phenol (1:3)	293.15 – 323.15	1.044 – 5.142	0.0029 – 0.0212		[72]
ChCl + phenol (1:2)	293.15 – 323.15	0.990 – 5.202	0.0027 – 0.0213		[72]
ChCl + lactic acid (1:2)	303.26 – 348.23	8.290 – 85.680	0.0248 – 0.0995		[73]
ChCl + urea (1:2)	303.15 – 343.15	2.990 – 95.100	0.0130 – 0.2530		[42,74]
ChCl + ethylene glycol (1:2)	303.15 – 343.15	2.360 – 63.230	0.0060 – 0.2160		[75]
ChCl + glycerol (1:2)	303.15 – 343.15	1.870 – 63.470	0.0050 – 0.2850		[43]
TPAB + formic acid (1:1)	298.15 – 318.15	2.100 – 32.625	0.0099 – 0.1694	0.0645 – 1.3060	This study
TPAB + formic acid (1:2)	298.15 – 318.15	1.650 – 35.225	0.0097 – 0.2180	0.0097 – 2.3340	This study

Table 4. Comparison of CO_2 solubility range of several well-known DESs with the DESs employed in this work.

DES (HBA + HBD)	Temperature range (K)	ΔH_{sol} ($kJ \cdot mol^{-1}$)	Ref
TBAC + decanoic acid (1:2) ($x_{CO_2} = 0.1$)	298–323	− 11.600	[66]
TOAB + decanoic acid (1:2) ($x_{CO_2} = 0.1$)	298–323	− 10.500	[66]
TOAC + decanoic acid (1:1.5) ($x_{CO_2} = 0.1$)	298–323	− 10.400	[66]
TOAC + decanoic acid (1:2) ($x_{CO_2} = 0.1$)	298–323	− 10.500	[66]
Selexol	294–357	− 13.400	[76]
Ethanol	298	− 12.800	[77]
Heptane	298	− 9.670	[77]
Benzene	298	− 9.340	[77]
MEA (30 wt %,$x_{CO_2} = 0.1$)	313	− 84.200	[77]
TPAB + formic acid (1:1)	298.15–318.15	− 13.164	This study
TPAB + formic acid (1:2)	298.15–318.15	− 16.175	This study

Table 5. The partial molar enthalpy of CO_2 solution in DESs employed in this study, other DESs, and various physical and chemical solvents across temperature and pressure ranges.

introduced an environmentally sustainable DES which is distinguished by its cost-effectiveness, higher absorption efficiency, and good recyclability.

Data availability

The datasets generated and/or analysed during the current study are available from the corresponding author on reasonable request.

Received: 22 April 2024; Accepted: 21 August 2024
Published online: 26 August 2024

References

1. Guo, Y. *et al.* Recent advances in potassium-based adsorbents for CO_2 capture and separation: A review. *Carbon Capture Sci. Technol.* **1**, 100011 (2021).
2. Nayak, N., Mehrotra, R. & Mehrotra, S. Carbon biosequestration strategies: A review. *Carbon Capture Sci. Technol.* **4**, 100065 (2022).
3. Davis, S. J., Caldeira, K. & Matthews, H. D. Future CO_2 emissions and climate change from existing energy infrastructure. *Science* **329**, 1330–1333 (2010).
4. Metz, B., Davidson, O., De Coninck, H., Loos, M. & Meyer, L. *IPCC Special Report on Carbon Dioxide Capture and Storage* (Cambridge University Press, 2005).
5. Karimi, M., Jodaei, A., Khajvandi, A., Sadeghinik, A. & Jahandideh, R. In-situ capture and conversion of atmospheric CO_2 into nano-$CaCO_3$ using a novel pathway based on deep eutectic choline chloride-calcium chloride. *J. Environ. Manag.* **206**, 516–522 (2018).
6. Zhang, Y. *et al.* CO_2 absorption and desorption performance by ChCl-MEA-PZ deep eutectic solvent aqueous solutions. *Sep. Purif. Technol.* **330**, 125275 (2024).
7. Nocito, F. & Dibenedetto, A. Atmospheric CO_2 mitigation technologies: Carbon capture utilization and storage. *Curr.Opin. Green Sustain. Chem.* **21**, 34–43 (2020).
8. Nowosielski, B., Warminska, D. & Cichowska-Kopczynska, I. CO_2 separation using supported deep eutectic liquid membranes based on 1, 2-propanediol. *ACS Sustain. Chem. Eng.* **11**, 4093–4105 (2023).
9. Gupta, S. Carbon sequestration in cementitious matrix containing pyrogenic carbon from waste biomass: A comparison of external and internal carbonation approach. *J. Build. Eng.* **43**, 102910 (2021).
10. Castro, M., Gómez-Díaz, D., Navaza, J. M. & Rumbo, A. Carbon dioxide capture by chemical solvents based on amino acids: Absorption and regeneration. *Chem. Eng. Technol.* **44**, 248–257 (2021).
11. Naderi, K., Foroughi, A. & Ghaemi, A. Analysis of hydraulic performance in a structured packing column for air/water system: RSM and ANN modeling. *Chem. Eng. Process. Process Intensif.* **193**, 109521 (2023).
12. He, X. *et al.* Analysis of the energy consumption in solvent regeneration processes using binary amine blends for CO_2 capture. *Energy* **270**, 126903 (2023).
13. Aronu, U. E. *et al.* Solubility of CO_2 in 15, 30, 45 and 60 mass% MEA from 40 to 120 °C and model representation using the extended UNIQUAC framework. *Chem. Eng. Sci.* **66**, 6393–6406 (2011).
14. Dutcher, B., Fan, M. & Russell, A. G. Amine-based CO_2 capture technology development from the beginning of 2013 a review. *ACS App. Mater. Interfaces* **7**, 2137–2148 (2015).
15. Zhang, R. *et al.* CuO modified KIT-6 as a high-efficiency catalyst for energy-efficient amine solvent regeneration. *Sep. Purif. Technol.* **300**, 121702 (2022).
16. Zheng, Y., Gao, L. & He, S. Analysis of the mechanism of energy consumption for CO_2 capture in a power system. *Energy* **262**, 125103 (2023).
17. Chen, L., Xiong, Y., Qin, H. & Qi, Z. Advances of ionic liquids and deep eutectic solvents in green processes of biomass-derived 5-hydroxymethylfurfural. *ChemSusChem* **15**, e202102635 (2022).
18. Greer, A. J., Jacquemin, J. & Hardacre, C. Industrial applications of ionic liquids. *Molecules* **25**, 5207 (2020).
19. Ptak, S., Zarski, A. & Kapusniak, J. The importance of ionic liquids in the modification of starch and processing of starch-based materials. *Materials* **13**, 4479 (2020).
20. Pandey, S. Analytical applications of room-temperature ionic liquids: A review of recent efforts. *Anal. Chim. Acta* **556**, 38–45 (2006).
21. Blanchard, L. A., Hancu, D., Beckman, E. J. & Brennecke, J. F. Green processing using ionic liquids and CO_2. *Nature* **399**, 28–29 (1999).
22. Bates, E. D., Mayton, R. D., Ntai, I. & Davis, J. H. CO_2 capture by a task-specific ionic liquid. *J. Am. Chem. Soc.* **124**, 926–927 (2002).
23. Huang, Y. *et al.* Preorganization and cooperation for highly efficient and reversible capture of low-concentration CO_2 by ionic liquids. *Angew. Chem. Int. Ed.* **56**, 13293–13297 (2017).
24. Chen, L. *et al.* Inexpensive ionic liquids:$[HSO_4]^-$-based solvent production at bulk scale. *Green Chem.* **16**, 3098–3106 (2014).
25. Elhenawy, S., Khraisheh, M., AlMomani, F. & Hassan, M. Key applications and potential limitations of ionic liquid membranes in the gas separation process of CO_2, CH_4, N_2, H_2 or mixtures of these gases from various gas streams. *Molecules* **25**, 4274 (2020).
26. Deetlefs, M. & Seddon, K. R. Assessing the greenness of some typical laboratory ionic liquid preparations. *Green Chem.* **12**, 17–30 (2010).
27. Romero, A., Santos, A., Tojo, J. & Rodríguez, A. Toxicity and biodegradability of imidazolium ionic liquids. *J. Hazard. Mater.* **151**, 268–273 (2008).
28. Tiano, M., Clark, R., Bourgeois, L. & Gomes, M. C. The dialkylcarbonate route to ionic liquids: Purer, safer, greener?. *Green Chem.* **25**, 2541–2558 (2023).
29. Naderi, K. *et al.* Modeling based on machine learning to investigate flue gas desulfurization performance by calcium silicate absorbent in a sand bed reactor. *Sci. Rep.* **14**, 954 (2024).
30. Abbott, A. P., Capper, G., Davies, D. L., Rasheed, R. K. & Tambyrajah, V. Novel solvent properties of choline chloride/urea mixtures. *Chem. commun.* **1**, 70–71 (2003).
31. Bučko, M. & Bajat, J. A review of the electrochemical corrosion of metals in choline chloride based deep eutectic solvents. *J. Electrochem. Sci. Eng.* **12**, 237–252 (2022).
32. García, G., Aparicio, S., Ullah, R. & Atilhan, M. Deep eutectic solvents: Physicochemical properties and gas separation applications. *Energy Fuels* **29**, 2616–2644 (2015).
33. Rezaee, M., Feyzi, F. & Dehghani, M. R. Extractive desulfurization of dibenzothiophene from normal octane using deep eutectic solvents as extracting agent. *J. Mol. Liq.* **333**, 115991 (2021).
34. Liu, Y. *et al.* Ionic liquids/deep eutectic solvents for CO_2 capture: Reviewing and evaluating. *Green Energy Environ.* **6**, 314–328 (2021).

35. Mirzaei, S., Shamiri, A. & Aroua, M. K. CO_2 absorption/desorption in aqueous single and novel hybrid solvents of glycerol and monoethanolamine in a pilot-scale packed bed column. *Energy Fuels* **34**, 8503–8515 (2020).
36. Wang, Y., Ren, S., Hou, Y. & Wu, W. Capture of acidic gases from flue gas by deep eutectic solvents. *Processes* **9**, 1268 (2021).
37. Zhang, N. *et al.* Highly efficient and reversible CO_2 capture by task-specific deep eutectic solvents. *Ind. Eng. Chem. Res.* **58**, 13321–13329 (2019).
38. Al-Bodour, A., Alomari, N., Gutiérrez, A., Aparicio, S. & Atilhan, M. High-pressure carbon dioxide solubility in terpene based deep eutectic solvents. *J. Environ. Chem. Eng.* **10**, 108237 (2022).
39. Ghanbari-Kalajahi, H. & Haghtalab, A. Vapor-liquid equilibrium of carbon dioxide solubility in a deep eutectic solvent (choline chloride: MDEA) and a mixture of DES with piperazine-experimental study and modeling. *J. Mol. Liq.* **375**, 121310 (2023).
40. Imteyaz, S. & Ingole, P. P. Comparison of physicochemical properties of choline chloride-based deep eutectic solvents for CO_2 capture: Progress and outlook. *J. Mol. Liq.* **376**, 121436 (2023).
41. Yu, J. *et al.* Deep eutectic solvents based on cyclodextrin–monoethanolamine for high-efficiency carbon dioxide capture under high temperature. *J. Environ. Chem. Eng.* **12**, 111625 (2023).
42. Li, X., Hou, M., Han, B., Wang, X. & Zou, L. Solubility of CO_2 in a choline chloride+ urea eutectic mixture. *J. Chem. Eng. Data* **53**, 548–550 (2008).
43. Leron, R. B. & Li, M.-H. Solubility of carbon dioxide in a eutectic mixture of choline chloride and glycerol at moderate pressures. *J. Chem. Thermodyn.* **57**, 131–136 (2013).
44. Sarmad, S., Xie, Y., Mikkola, J.-P. & Ji, X. Screening of deep eutectic solvents (DESs) as green CO_2 sorbents: From solubility to viscosity. *New J. Chem.* **41**, 290–301 (2017).
45. Zhang, K. *et al.* Efficient and reversible absorption of CO_2 by functional deep eutectic solvents. *Energy Fuels* **32**, 7727–7733 (2018).
46. Yan, H. *et al.* Superbase ionic liquid-based deep eutectic solvents for improving CO_2 absorption. *ACS Sustain. Chem. Eng.* **8**, 2523–2530 (2020).
47. Li, M., Zhu, C., Fu, T., Gao, X. & Ma, Y. Effect of water on amine-based deep eutectic solvents (choline chloride+ monoethanolamine): Structure and physicochemical properties. *J. Environ. Chem. Eng.* **10**, 106952 (2022).
48. Mirza, N. R. *et al.* Viscosities and carbon dioxide solubilities of guanidine carbonate and malic acid-based eutectic solvents. *J. Chem. Eng. Data* **62**, 348–354 (2017).
49. Abdrabou, H. K. *et al.* Experimental investigation of novel ternary amine-based deep eutectic solvents for CO_2 capture. *PLoS One* **18**, e0286960 (2023).
50. Wasserscheid, P. & Welton, T. M. *Ionic Liquids in Synthesis* (Wiley Online Library, 2008).
51. Li, Z. *et al.* Absorption of carbon dioxide using ethanolamine-based deep eutectic solvents. *ACS Sustain. Chem. Eng.* **7**, 10403–10414 (2019).
52. Song, X. *et al.* Carbon dioxide separation performance evaluation of amine-based versus choline-based deep eutectic solvents. *Renew. Sustain. Energy Rev.* **184**, 113499 (2023).
53. Trivedi, T. J., Lee, J. H., Lee, H. J., Jeong, Y. K. & Choi, J. W. Deep eutectic solvents as attractive media for CO_2 capture. *Green Chem.* **18**, 2834–2842 (2016).
54. Peng, D.-Y. & Robinson, D. B. A new two-constant equation of state. *Ind. Eng. Chem. Fundam.* **15**, 59–64 (1976).
55. Renon, H. & Prausnitz, J. M. Local compositions in thermodynamic excess functions for liquid mixtures. *AIChE J.* **14**, 135–144 (1968).
56. Hedayati, A. & Feyzi, F. CO_2-binding organic liquids comprised of 1, 1, 3, 3-tetramethylguanidine and alkanol for postcombustion CO_2 capture: Water inhibitory effect of amine promoters. *ACS Sustain. Chem. Eng.* **8**, 7909–7920 (2020).
57. Najafloo, A., Zoghi, A. T. & Feyzi, F. Measuring solubility of carbon dioxide in aqueous blends of N-methyldiethanolamine and 2-((2-aminoethyl) amino) ethanol at low CO_2 loadings and modelling by electrolyte SAFT-HR EoS. *J. Chem. Thermodyn.* **82**, 143–155 (2015).
58. Zoghi, A. T., Feyzi, F. & Zarrinpashneh, S. Experimental investigation on the effect of addition of amine activators to aqueous solutions of N-methyldiethanolamine on the rate of carbon dioxide absorption. *Int. J. Greenh. Gas Control* **7**, 12–19 (2012).
59. Zoghi, A. T., Feyzi, F. & Zarrinpashneh, S. Equilibrium solubility of carbon dioxide in a 30 wt.% aqueous solution of 2-((2-aminoethyl) amino) ethanol at pressures between atmospheric and 4400 kPa: An experimental and modelling study. *J. Chem. Thermodyn.* **44**, 66–74 (2012).
60. Ibrahim, M., Nada, A. & Kamal, D. E. Density functional theory and FTIR spectroscopic study of carboxyl group. *Indian J. Pure Appl. Phys.* **43**, 911–917 (2005).
61. Ke, P. *et al.* Preparation of quaternary ammonium salt-modified chitosan microspheres and their application in dyeing wastewater treatment. *ACS Omega* **5**, 24700–24707 (2020).
62. Jincheng, W., Xiaoyu, Z., Wenli, H., Nan, X. & Xingchen, P. Synthesis of hyper-branched quaternary ammonium salt and its application into montmorillonite. *Powder Technol.* **221**, 80–89 (2012).
63. Hore, P. J. *Nuclear Magnetic Resonance* (Oxford University Press, 2015).
64. Rolle, F. & Sega, M. Use of FTIR spectroscopy for the measurement of CO_2 carbon stable isotope ratios. in *19th International Congress of Metrology (CIM2019)*. 05002 (EDP Sciences).
65. Stuart, B. H. *Infrared Spectroscopy: Fundamentals and Applications* (John Wiley & Sons, 2004).
66. Zubeir, L. F., Van Osch, D. J., Rocha, M. A., Banat, F. & Kroon, M. C. Carbon dioxide solubilities in decanoic acid-based hydrophobic deep eutectic solvents. *J. Chem. Eng. Data* **63**, 913–919 (2018).
67. The MathWork, Inc. MATLAB version: 1.0.0.1 (R2022b). https://www.mathworks.com (2022).
68. Gu, Y., Hou, Y., Ren, S., Sun, Y. & Wu, W. Hydrophobic functional deep eutectic solvents used for efficient and reversible capture of CO_2. *ACS Omega* **5**, 6809–6816 (2020).
69. Jiang, B. *et al.* Superbase/acylamido-based deep eutectic solvents for multiple-site efficient CO_2 absorption. *Energy Fuels* **33**, 7569–7577 (2019).
70. Deng, D., Jiang, Y., Liu, X., Zhang, Z. & Ai, N. Investigation of solubilities of carbon dioxide in five levulinic acid-based deep eutectic solvents and their thermodynamic properties. *J. Chem. Thermodyn.* **103**, 212–217 (2016).
71. Zubeir, L. F., Held, C., Sadowski, G. & Kroon, M. C. PC-SAFT modeling of CO_2 solubilities in deep eutectic solvents. *J. Phys. Chem. B* **120**, 2300–2310 (2016).
72. Li, G., Deng, D., Chen, Y., Shan, H. & Ai, N. Solubilities and thermodynamic properties of CO_2 in choline–chloride based deep eutectic solvents. *J. Chem. Thermodyn.* **75**, 58–62 (2014).
73. Francisco, M., van den Bruinhorst, A., Zubeir, L. F., Peters, C. J. & Kroon, M. C. A new low transition temperature mixture (LTTM) formed by choline chloride+ lactic acid: Characterization as solvent for CO_2 capture. *Fluid Phase Equilib.* **340**, 77–84 (2013).
74. Leron, R. B., Caparanga, A. & Li, M.-H. Carbon dioxide solubility in a deep eutectic solvent based on choline chloride and urea at T= 303.15–343.15 K and moderate pressures. *J. Taiwan Inst. Chem. Eng.* **44**, 879–885 (2013).
75. Leron, R. B. & Li, M.-H. Solubility of carbon dioxide in a choline chloride–ethylene glycol based deep eutectic solvent. *Thermochim. Acta* **551**, 14–19 (2013).
76. Xu, Y., Schutte, R. P. & Hepler, L. G. Solubilities of carbon dioxide, hydrogen sulfide and sulfur dioxide in physical solvents. *Can. J. Chem. Eng.* **70**, 569–573 (1992).
77. Wilhelm, E. & Battino, R. Thermodynamic functions of the solubilities of gases in liquids at 25. deg. *Chem. Rev.* **73**, 1–9 (1973).

Author contributions

A.A.M.: experimental work, methodology, conceptualization, data curation, formal analysis, investigation, writing original draft. F.F.: supervision, conceptualization, methodology, resources, data curation, review and editing. M.R.: methodology, data curation, conceptualization. All authors reviewed the manuscript.

Competing interests

The authors declare no competing interests.

Additional information

Correspondence and requests for materials should be addressed to F.F.

Reprints and permissions information is available at www.nature.com/reprints.

Publisher's note Springer Nature remains neutral with regard to jurisdictional claims in published maps and institutional affiliations.